GEOFIZIKA VOL. 30 2013

Original scientific paper
UDC 551.581.1, 551.588.7

Recent climate trends and future scenarios along the Egyptian Mediterranean coast

Mohamed Shaltout [1, 2], *Ahmed El Gindy* [1] *and Anders Omstedt* [2]

[1] University of Alexandria, Faculty of Science, Department of Oceanography, Alexandria, Egypt

[2] University of Gothenburg, Department of Earth Sciences, Göteborg, Sweden

Received 19 March 2012, in final form 3 January 2013

This paper analyses the present Egyptian Mediterranean coast (EMC) climate and the response of its climate variables to global changes. First, the accuracy of the ERA-Interim dataset (1979–2010) for the studied region is examined by comparing these data with available independent observations. Second, the qualities of six global climate models (GCMs), together with the ensemble mean of multiple model realisations of the A1B scenario, are examined by comparing these with the ERA-Interim dataset. Finally, GCM simulations are used to describe the uncertainties in future climate change along the EMC.

The results indicate that the observations are in good agreement with the ERA-Interim data. The data for the EMC, 1979–2000, display a significant positive trend for 2-m air temperature together with significant negative trends for total precipitation and sea level pressure. The climate model that best describes the present EMC climate is the CGCM 3.1 model, which is used to describe the future climate of the study area. The CGCM 3.1 model indicates that the EMC area will experience significant warming, substantial droughts, and a weak decrease in sea level pressure in the end of the current century.

Keywords: Mediterranean Sea, Egypt, air temperature, precipitation, sea level pressure, climate, trend analysis, climatic models

1. Introduction

The Egyptian Mediterranean coast and its adjacent area (EMC), which extends from 25° to 34.5° East and 30° to 33° North (Fig. 1), represents an important environmental resource for tourism, farming, and fisheries. Egypt is especially vulnerable to the effects of climate change due to its high population density and inability to deal with extreme weather events. Moreover, the EMC is exposed to sea level rise and land subsidence. Consequently, the EMC is regarded as an extreme hotspot of climate vulnerability, for example, by the Intergovernmental Panel on Climate Change (IPCC). Designing appropriate adapta-

tion and mitigation solutions calls for close study of how climate change will affect the EMC, which is the aim of the present paper.

Some earlier relevant studies are available. Hafez and Hasanean (2000) demonstrated that the amount of winter precipitation along the northern coast of Egypt changed dramatically over the 1961–1999 period. They found that the wettest (driest) winter was in 1983 (1979) and that the precipitation regime differed from the eastern (higher precipitation) to the western (lower precipitation) parts of Egypt. Scavia et al. (2002) demonstrated that increasing air temperature together with changed patterns of precipitation and wind are important climate issues and are also responsible for sea level changes. Hasanean (2004a) found a negative relationship between the North Atlantic Oscillation Index and winter air temperature over Egypt; he also found that the coefficient of variation (COV) of air temperature is 4–11% in winter over Egypt. The annual amount of Mediterranean precipitation has been declining since the mid twentieth century (Hasanean, 2004b). Domroes and El-Tantawi (2005) stated that Egypt's annual mean air temperature increased by 0.6 °C decade^{-1} from 1971 to 2000, most markedly in the summer. Houghton et al. (2001) demonstrated that the frequency of projected hot days in the twenty-first century would increase, as would the incidence of droughts. Agrawala et al. (2004), using data from 17 GCMs but only one emission level scenario (i.e., the B2 scenario), estimated that Egypt's annual average temperature and precipitation could change by +2.4 °C and –13.2%, respectively, by 2100. Arnell (2004) stated that the projected global warming in the current century for the B1, A1B, and A2 scenarios would be 1.7, 2.7, and 3.5 °C, respectively. The IPCC (2007) projected that the global surface air temperature would increase by 1.8–4 °C by 2100, with the greatest warming occurring in high-latitude areas. Alcamo et al. (2007) projected that annual mean surface air temperatures in the northern Mediterranean region under the A1B scenario would rise by 2.2–5.1 °C. The Mediterranean region is also projected to experience a substantial increase in droughts (IPCC, 2007), and the UNDP (2007) found that expected precipitation rates will decrease in Egypt. For the Mediterranean region, global and regional climate models have projected a general negative precipitation trend in the current century, subject to clear spatial and seasonal variability (Giorgi and Lionello, 2008; Goubanova and Li, 2007). Kjellström et al. (2011) suggested that identifying the uncertainty of future climate change would require multiple GCM realisations with several scenarios.

The European Centre for Medium-Range Weather Forecasts (ECMWF) datasets (i.e., ERA-40 and ERA-Interim) were recently used for climate studies (Berrisford et al., 2011; Douglas et al., 2009; Kaltenbrock et al., 2009). The total precipitation values from the ECMWF datasets were in good agreement with observations from the Mediterranean area (Accadia et al., 2005; Cherubini et al., 2002). ECMWF data for the EMC area, however, have not previously been examined in much detail.

In 1996, the IPCC released the Special Report on Emissions Scenarios (SRES). The SRES scenarios cover a wide variety of the main driving forces of future emissions, ranging from demographic to technological and economic developments. They also cover the range of emissions of all relevant species of greenhouse gases (GHGs) and sulphur, together with their driving forces (IPCC, 2000). The present study examines three SRES emission scenarios, the A1B, A2, and B1 scenarios.

This paper examines the EMC climate, first analysing observations and ERA-Interim reanalysis values for the EMC. Then, 32 years (1979–2010) of reanalysis data for the area, capturing air temperature at 2 m above sea level (T_{2m}), total precipitation (P), and sea level pressure (SLP), are studied. Finally, future projections of the EMC climate up to 2200 are analysed using various global climatic scenarios.

2. Materials and methods

This paper discusses current trends (1981–2010) and future scenarios (up to 2200) for the EMC climate, including the variables T_{2m}, P, and SLP. These variables display large monthly, seasonal, inter-annual, and long-term variability. To understand the dynamics of these variables and their responses to global climate change, several data sources have been used, encompassing observation and reanalysis data (Fig. 1) together with the results of six GCMs' realisations.

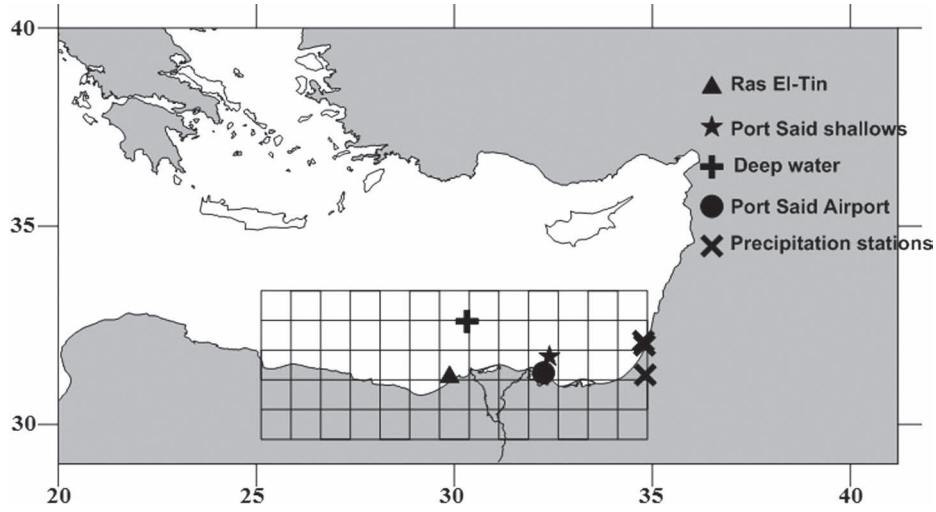

Figure 1. Sites of observations and ERA-Interim gridded data in the Egyptian Mediterranean study area.

2.1. Data

2.1.1. Observations

The direct observation time series analysed in the present study include:

– Observed three-hourly T_{2m} and *SLP* at the Ras El-Tin station (31.20° N, 29.88° E) from 1 January1998 to 31 December 2000 obtained from the Egyptian army

– Observed hourly T_{2m} and *SLP* at the Port Said shallow-water station (31.71° N, 32.4° E; 45-m water depth) from 1 February 1999 to 24 February 2000 obtained from Fugro Global Environmental and Ocean Sciences (Fugro GEOS), which used an Aanderaa automatic meteorological station

– Observed hourly T_{2m} and *SLP* over deep water (32.60° N, 30.32° E; 1750-m water depth) from 1 May 1999 to 30 April 2000 obtained from Fugro GEOS, which used an Aanderaa automatic meteorological station

– Observed daily T_{2m} and *SLP* at Port Said Airport (31.3° N, 32.25° E) from 1997 to 2009 (http://www.wunderground.com)

– Observed daily *P* at Tel Aviv (32.10° N, 34.77° E), Bet Dagan (32.00° N, 34.80° E), and Beer Sheva (31.25° N, 34.82° E) from 1 January 1979 to 31 December 2004. These data were extracted from the KNMI Climate Explorer (climexp.knmi.nl)

2.1.2. Reanalysis

Reanalyzed gridded data on T_{2m}, *SLP*, and *P* for the EMC were extracted from the ECMWF data server for meteorological data (i.e., ERA-Interim). These data have a 3-h temporal resolution and a spatial resolution of 0.75° × 0.75° over the 1981–2000 period.

2.2. Results of six global climate models

GCMs are continuously improving and can provide projections based on various forcing assumptions; however, their resolution is too coarse for the regional and local scales (Räisänen and Alexandersson, 2003). The present paper examines six GCMs to study the effects on the EMC of anthropogenic climate change due to increased greenhouse gas emissions. Monthly average GCM simulation results for T_{2m}, *SLP*, and *P* were extracted from the KNMI Climate Explorer (climexp.knmi.nl), in which runs for three emission scenarios (i.e., A1B, A2, and B1) are available. For each emission scenario, there were one to six realisations of individual GCMs differing only in the initial conditions (Tab. 1).

2.3. Methodology

Analysing recent climate trends and future scenarios for T_{2m}, *P*, and *SLP* call for various steps. The first step is to analyse the present climate system us-

Table 1. Simulations of various global climate models.

GCM name, year	Organisation	Emission scenario, number of realisations	Simulation period	Horizontal resolution, relevant reference
BCCR-BCM2.0 (BCM), 2005	Bergen Climate Model (Norway)	A1B, 1	1850–2100	1.9° × 1.9° (Deque et al., 1994)
CGCM3.1 (T47), 2005	Canadian Centre for Climate Modelling and Analysis (Canada)	A1B, 4	1850–2200	2.8° × 2.8° (Flato, 2005)
		B1, 4	2001–2200	
		A2, 1	2001–2100	
CNRM-CM3, 2004	Centre National de Recherches Météorologiques (France)	A1B, 1	1860–2200	1.9° × 1.9° (Terray et al., 1998)
		A2, 1	2000–2100	
GFDL CM2.1, 2005	Geophysical Fluid Dynamics Laboratory climate model, NOAA (USA)	A1B, 1	1861–2300	2.5° longitude, 2.0° latitude (Delworth et al., 2006)
		B1, 1	2001–2100	
		A2, 1	2001–2300	
ECHAM5/MPI-OM, 2005	Max-Planck Institute for Meteorology Climate Model, (Germany)	A1B, 3	1861–2200	1.9° × 1.9° (Jungclaus et al., 2006)
		B1, 2	2001–2100	
		A2, 2	2001–2300	
CCSM3.0, 2005	National Centre for Atmospheric Research (NCAR) Community Climate System Model (USA)	A1B, 6	1870–2350	1.4° × 1.4° (Collins et al., 2006)
		A2, 3	2000–2100	

ing available observations, which will teach us how the present climate is changing in the region. The second step is to correlate local observations with independent gridded datasets (ERA-Interim data). ERA-Interim data, based on both observed and modelled information, capture the climate conditions on a larger horizontal scale. The observations used in our analysis are independent of the observations used in the gridded dataset's numerical model. If the gridded data reasonably represent the observations, they can be used to better characterize the climate that the models simulate (the third step). The fourth step is to use ERA-Interim data and to evaluate how well the climate models describe present climate conditions. Based on this evaluation, future climate change uncertainties can be described as related to emissions, boundary conditions, and the climate model used.

2.3.1. The gridded ERA-Interim dataset

Direct comparisons of the three-hour and daily time steps between observations and the ERA-Interim gridded dataset are used to test the accuracy of ERA-Interim data. A direct comparison using regression analysis (the constant is zero) to examine the similarity between both datasets yields the correlation coefficient (R), standard error (SE), and number of observations (n). The regression equation slope was tested to check the similarity of the two independent datasets, i.e., whether or not the slope is significantly equal to one, and hence to conclude whether ERA-Interim data can be used in the analysis or whether they must be calibrated by local observations. The t- and f-tests are used to confirm whether the observations and reanalysis datasets come from the same population, i.e., do they display equal means and variances. A coefficient of variation (COV) for each ERA-Interim grid is calculated as $100\frac{\text{standard deviation}}{\text{mean}}$ to indicate the weather variable stability, which increased with decreasing COV.

A linear trend analysis based on the ERA-Interim database from 1979 to 2010 is used to characterize the climate change in the study area. For precipitation analysis over the whole study area, trends in the number of significant precipitation days ($P \geq 0.1$ mm day^{-1}) are described over three rain intensity classes, depending on the mean and standard deviation. All linear trends analysis has been tested for significance using t-test.

Finally, links between the North Atlantic Oscillation (NAO), captured by the NAO Index, and winter changes in T_{2m}, P, and SLP are investigated. The NAO Index is extracted from the NOAA National Weather Service database (http://www.cpc.ncep.noaa.gov/products/precip/CWlink/pna/nao_index.html); a positive sign indicates cold, dry winters in the Mediterranean region while a negative sign indicates warm, wet winters (Fig. 2).

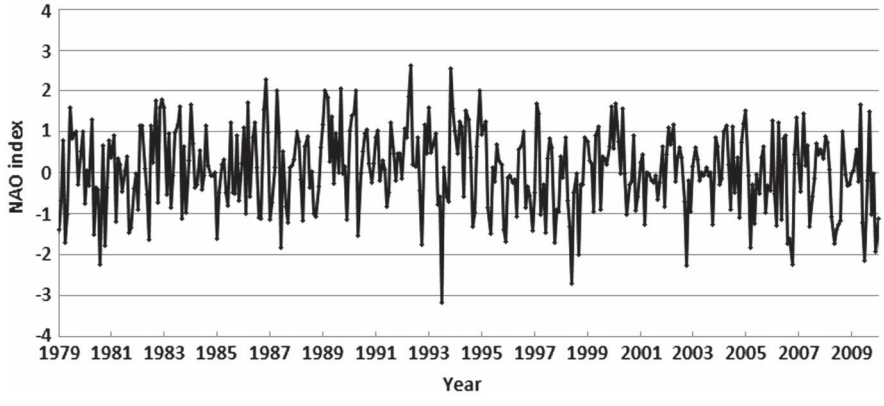

Figure 2. Monthly time series of the North Atlantic Oscillation (NAO) Index.

2.3.2. Climate model results over the study area

The results of the six GCMs' realisations of the A1B scenario for the 1981–2000 period were examined using ERA-Interim data. Next, realisations that reasonably simulated the current climate were used to identify the uncertainties in the future EMC climate.

Monthly and annual averages are calculated for a 20-year control period, 1981–2000, to compare the GCM and ERA-Interim data. The only GCM scenario used in this step is the A1B scenario. Direct bias (GCM – ERAInterim) is used to test T_{2m}, while bias percentage $\%\frac{\text{GCM}-\text{ERAInterim}}{\text{ERAInterim}}$ is used to examine total precipitation. Kjellström et al. (2011) described a technique for measuring the agreement between the reanalysis and GCM-simulated results. This technique is based on calculating the explained variance (E), defined as $E = 1 - \frac{\sigma^2_{diff}}{\sigma^2_{res}}$, where σ^2_{diff} is the variance of the difference between the simulated and reanalysis long-term averages, while σ^2_{res} is the variance of the long-term reanalysis averages. When E is close to one, this indicates good agreement, whereas small or negative values of E indicate poor agreement.

Thirty-year seasonal averages for T_{2m}, P, and SLP for 2011–2040 to 2161–2190 are calculated to describe future uncertainty scenarios. Only GCM realisations that reasonably simulate the current EMC climate are used to illustrate the uncertainty of the future climate based on the A1B, A2, and B1 scenarios.

3. Results

3.1. Observations and reanalysis

In this section, three weather variable characteristics (i.e., T_{2m}, P, and SLP) are described using the observations. In addition, the feasibility of using ERA-Interim reanalysis data in describing the study area climate is investigated by means of direct comparison between observed and reanalysis values.

The three weather variable characteristics have been carefully validated against observations from the stations. The results of this comparison are presented in Tab. 2, which indicates the following:

Observed T_{2m} values agreed well with ERA-Interim data, with a small annual bias of 0–0.1 °C. The correlations over sea (0.98–0.99) are higher than over land stations (0.9–0.96).

Twenty-six years (1979–2004) of data on average daily observed and reanalysis precipitation (P) over the Middle Eastern grid of the study area (i.e., North Israel, Tel Aviv, and Bet Dagan) were significantly correlated, with no annual bias. Thirty-two years (1979–2010) of comparable data for south Israel (Beer Sheva) were significantly correlated, with an annual bias of 0.21 mm day^{-1}.

Table 2. Regression analysis of observed and reanalysed weather variables: constant = 0, n = number of observations, R = correlation coefficient, and SE = standard error; significance of slope (= 1) represents the difference between the slope and unity.

	Station		Slope	Significance of slope (=1)	*n*	*R*	*SE* (°C)	Mini-mum	Maxi-mum	Annual average ± standard deviation
2-m air temperature (°C)	Ras El-Tin	Observed	1.005	Yes	11687	0.90	1.8	7.6	39.4	20.8 ± 4.8
		Reanalysis						10.2	28.8	20.8 ± 4.4
	Port Said shallow water	Observed	0.994	Yes	2594	0.98	0.85	8.4	27.7	19.7 ± 4
		Reanalysis						8.7	29.5	19.8 ± 4.2
	Deep water	Observed	0.993	Yes	2878	0.99	0.6	8.8	28.26	20.6 ± 4.38
		Reanalysis						9.7	28.8	20.7 ± 4.2
	Port Said airport	Observed	1.007	Yes	4331	0.96	1.4	7	34	21.2 ± 4.9
		Reanalysis						10.3	29.1	21.15 ± 4.4
Precipitation (mm day^{-1})	North Israel (Tel Aviv and Bet Dagan)	Observed	0.85	Yes	9280	0.55	3.4	0	44.3	1.46 ± 5.3
		Reanalysis						0	80.4	1.41 ± 3.8
	South Israel (Beer Sheva)	Observed	0.86	Yes	10634	0.48	2.4	0	55.1	0.6 ± 2.9
		Reanalysis						0	62.6	0.81 ± 2.4
Sea level pressure (mbar)	Ras El-Tin	Observed	1	Yes	11687	0.999	1.5	991	1032	1014 ± 5
		Reanalysis						988	1030	1014 ± 5
	Port Said shallow water	Observed	1	Yes	2594	1	0.7	1001.2	1028.4	1014.9 ± 5
		Reanalysis						1000.5	1028.4	1015 ± 5.1
	Deep water	Observed	1	Yes	2878	0.999	1	997.1	1026.7	1014.4 ± 5.3
		Reanalysis						996.6	1027.7	1014.3 ± 5.5
	Port Said airport	Observed	1	Yes	4335	1	0.6	999	1031	1013.5 ± 4.8
		Reanalysis						997	1030.8	1013.5 ± 5

Reanalysis sea level pressure (*SLP*) closely matched the observations, with a negligible annual bias for all observation stations.

The statistical tests (*t*- and *f*-tests) indicated that observed and reanalysis T_{2m}, *P*, and *SLP* values form two equal distributions of mean and variance at a 99% significance level. Regression slopes (at zero constant) between the reanalysis and observed data are close to one for the studied variables at the observation stations. The ERA-Interim dataset therefore seems to realistically describe the EMC climate.

3.2. Trend analysis

In this section, 33 years of ERA-Interim Reanalysis data for three weather variables (i.e., T_{2m}, *P*, and *SLP*) are subject to trend analysis.

Average and trend statistics for the three weather components over the EMC captured by ERA-Interim reanalysis data are shown in Fig. 3. Figs. 4–6 show seasonal time series for different weather variables.

The annual average values of T_{2m} and the corresponding positive linear trends are spatially distributed; for example, air temperature increases moving inland from the coast. Approximately 92% of the study areas have a T_{2m} linear trend of 0.40–0.57 °C decade^{-1}; all the oceanic study area lies in this range (Fig. 3a). The annual *COV* of air temperature ranges spatially from 20.9% to 41.5%

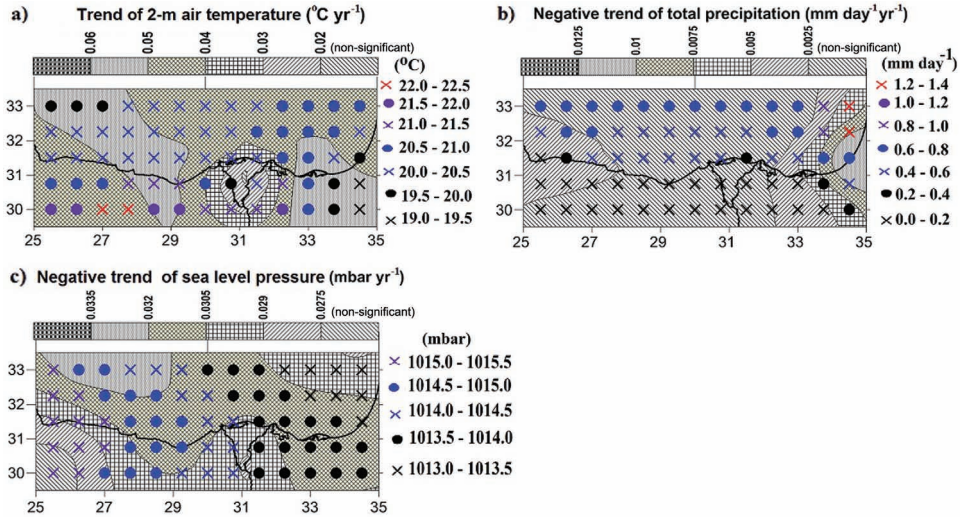

Figure 3. Annual average (right legend) and trend (upper legend) statistics for (a) 2-m air temperature, (b) total precipitation, and (c) sea level pressure over the Egyptian Mediterranean coast using ERA-Interim reanalysis data.

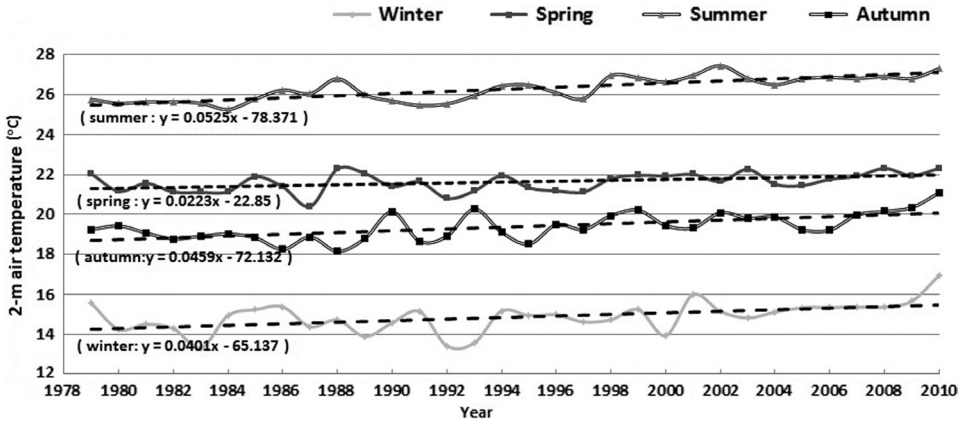

Figure 4. Four seasonal time series and linear trends (black dashed line) for 2-m air temperature over the Egyptian Mediterranean coast region. Linear trend line equations for each season are presented on the left-hand side.

with an average value of 26.2%. The annual *COV* of T_{2m} changes substantially in the latitudinal direction (i.e., it increases moving inland), but very weakly in the longitudinal direction (data not shown). This means that T_{2m} is less variable over sea than it is over land. In general, relatively cool months occur from December to February, though they occur in only January and February after 1994. This may indicate a climate shift over the studied region. Years with much cooler winters over the EMC were 1983, 1992, 1993, 1989, and 2000 (< 14.1 °C; winter mean – winter standard deviation), while much warmer winters occurred in 2001, 2009, and 2010 (> 15.5 °C; winter mean + winter standard deviation). Air temperature at 2 m height displayed seasonal variability, with average values varying from 14.8 °C (winter) to 26.5 °C (summer) and linear increasing trends ranging from 0.024 °C decade^{-1} (spring) to 0.52 °C decade^{-1} (summer), as seen in Fig. 4. Moreover, *COV* also displayed seasonal variability over the whole study area, ranging from 9.6% (summer) to 19.9% (autumn); the seasonal *COV* variability agrees with the results of Hasanean (2004a) and Hasanean and Abdel Basset (2006).

Annual average values of P (0.053–1.394 mm day^{-1}) displayed a spatial distribution with increasing values towards the north and east. Total precipitation annual *COV* is high (> 100%) for each grid, which means that total precipitation varies considerably. The annual trend in P was also spatially distributed, varying between non-significant and negative (i.e., –0.137 mm day^{-1} decade^{-1}). More than 63% of the study area has non-significant precipitation trends, highly significant precipitation trends (i.e., > 0.05 mm day^{-1} decade^{-1}) being found only in the eastern part of the study area (Fig. 3b). Overall, extremely wet winters occurred in 1992, 1991, 1983, 1988, 2003, and 1996 (> 1.13 mm day^{-1}; winter mean

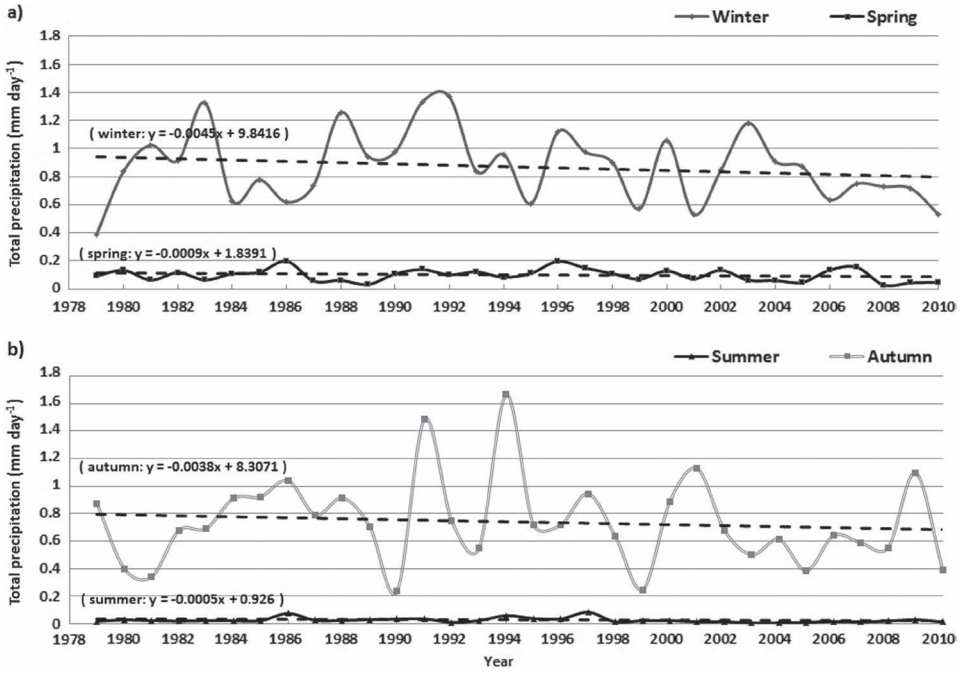

Figure 5. Seasonal time series and linear trends (black dashed line) for total precipitation over the Egyptian Mediterranean coast region in (a) winter and spring and (b) summer and autumn. Linear trend line equations for each season are presented on the left-hand side.

+ winter standard deviation), while extremely dry winters occurred in 1979, 2001, 2010, 1999, and 1995 (< 0.61 mm day^{-1}; winter mean – winter standard deviation). There was an obvious (Fig. 5) seasonal distribution for average P values (0.025–0.870 mm day^{-1}) and trends (non-significant to –0.045 mm day^{-1} decade^{-1}), in agreement with Hasanean (2004b). The maximum annual average value and trend of P are observed in winter, while the minimum value and trend are observed in summer.

Generally, wet days (P > 0.1 mm day^{-1}) are divided into three groups: (1) low wet days (0.1 < P < 1.5 mm day^{-1}; daily mean + daily standard deviation), (2) moderate wet days (1.5 < P < 4 mm day^{-1}; daily mean + 3 × daily standard deviation), and (3) high wet days (P > 4 mm day^{-1}). The annual total number of low wet days (mean = 85.7 days) decreased by 20.4 days from 1979 to 2010. Over the same period, the annual total number of moderate wet days (mean = 22.3 days) decreased by 4.5 days, while the annual total number of high wet days (mean = 9.5 days) decreased by one day. The study area is therefore safe from reservoir breakage and floods, while it is expected to suffer from drought in the future.

The average annual *SLP* values (1013.12–1015.47 mbar) were spatially distributed, generally decreasing eastward (Fig. 3c). The *COV* of *SLP* is annually homogenous over the study area (i.e., 0.5%), meaning that *SLP* is a highly stable variable. The annual linear negative trend of *SLP* displayed an obvious spatial distribution, i.e., it was non-significant over the south-west of the study area but reached to –0.33 mbar decade^{-1} over the north-west of the study area. *SLP* displayed seasonal variability, with average values ranging from 1009.8 mbar (summer) to 1017.4 mbar (winter), and a linear trend ranging from non-significant (winter) to –0.52 mbar decade^{-1} (summer), as shown in Fig. 6. This seasonal variability of *SLP* average values may be due to the inverse relationship between T_{2m} and *SLP*. In addition, the *COV* of *SLP* displayed seasonal variability ranging from 0.28% (summer) to 0.48% (winter).

Generally, T_{2m}, *P*, and *SLP* are significantly related to the NAO Index in winter, cooler winters being related to positive NAO Index values and warmer winters to negative ones. The correlation coefficient between the winter NAO Index and the T_{2m} index is significant (R = –0.49, n = 32, level of significance > 99%), which agrees with Hasanean's (2004a) results. High (low) winter precipitation occurred with positive (negative) NAO Index values. The winter NAO

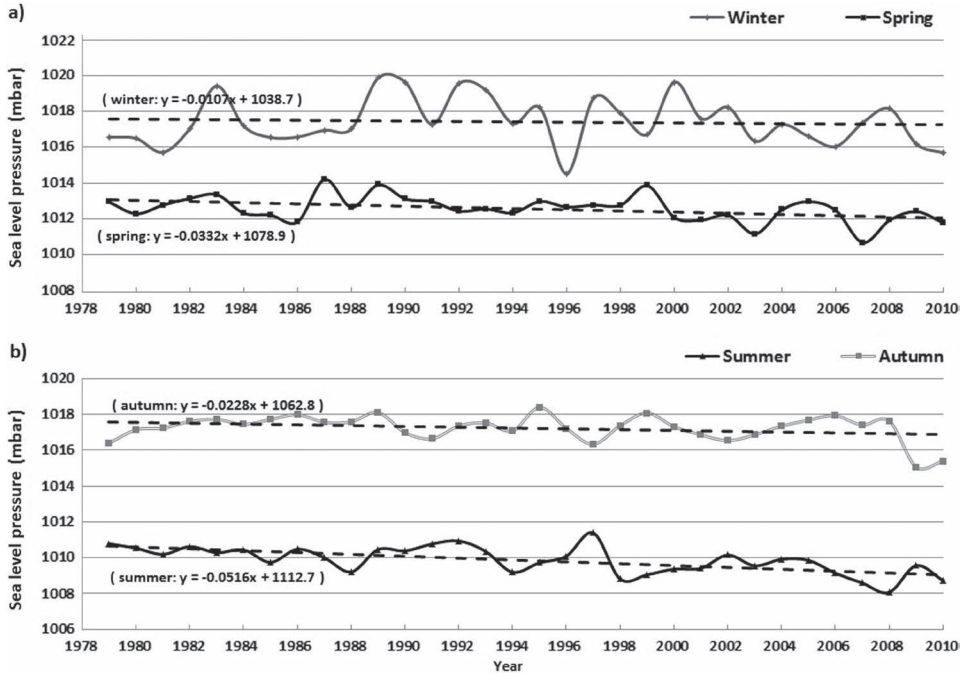

Figure 6. Seasonal time series and linear trends (black dashed lines) for sea level pressure over the Egyptian Mediterranean coast region for (a) winter and spring and (b) summer and autumn. Linear trend line equations for each season are presented on the left-hand side.

Index and P are significantly correlated (R = 0.33, n = 32, level of significance = 94%), as are the winter NAO Index and *SLP* (R = 0.73, n = 32, level of significance > 99%).

3.3. Scenarios

In this section, the results of six GCMs with different scenarios and initial conditions (realisations) are investigated for T_{2m}, P, and *SLP*.

Control climate period (1981–2000)

Tab. 3 shows the performance of 16 realisations of the A1B scenario. The ensemble mean of all 16 realisations of the A1B scenario (EMR16-A1B) is computed and presented for each variable in the last row of Tab. 3. The results in Tab. 3 are subjected to the t-test to determine whether the model-estimated values are significantly lower or higher than the ERA-Interim reanalysis values.

In the case of T_{2m}, most GCM simulations (except the CNRM-CM3 model) insignificantly underestimate/overestimate monthly and annual T_{2m} with respect to ERA-Interim data. The ensemble mean of all T_{2m} realisations indicated insignificantly lower estimates of monthly T_{2m}, ranging from 0.1 °C lower (July and August) to 1.5 °C lower (April), with the annual estimate being 1 °C lower.

For P, the CGCM3.1 model's various realisations (i.e., i1–i4) insignificantly underestimated/overestimated the annual mean P when compared with the ERA-Interim data, while the other GCMs exhibit significant departures from the ERA-Interim data. The ensemble mean of all P realisations indicated an insignificant annual underestimation of approximately 21% in the rainy months from October to March (range, 13–38%) and 34–202% overestimation in the rest of the year. GCM performance varies considerably from month to month.

For *SLP*, the E value is used to examine the agreement between simulated and ERA-Interim data. The best-fit *SLP* realisations for the study area during the control period (annual E > 0.6) are four realisations of CGCM3.1 and three realisations of ECHAM5/MPI-OM together with BCM, while the ensemble mean of all *SLP* realisations is in good agreement with the ERA-Interim data (annual E = 0.8). For most realisations, there is poor (reasonable) monthly (annual) agreement between simulated realisations and ERA-Interim data. Generally, the various GCM realisations overestimate *SLP* by 2–3 mbar compared with ERA-Interim reanalysis data (not shown).

Generally, EMR16-A1B produces a better annual simulation of *SLP* than do individual simulations; moreover, EMR16-A1B reasonably simulates T_{2m} and P. This indicates that the averaging cancels out some of the individual simulation errors.

Consequently, all CGCM3.1 model realisations (i.e., i1–i4) for the A1B scenario, together with the EMR16-A1B simulations, are the best simulations describing the control period climate and would be usable for studying future climate uncertainties over the EMC.

Table 3. Performance of various GCMs in the control period (1981–2000): only the A1B scenario is used, but with different initial conditions (i); EMR16-A1B = ensemble mean of all 16 realisations of the A1B scenario.

a)	Model	Realisation	Jan	Feb	Mar	Apr	May	June	Jul	Aug	Sep	Oct	Nov	Dec	Annual
Temperature (Bias, °C)	BCM	A1B-i1	1.6	0.7	0.0	–1.8	–2.8	–2.6	–1.4	–0.3	–0.3	0.0	1.0	1.5	–0.4
	CGCM3.1	A1B-i1	–2.8	–1.6	–1.1	–0.6	–0.2	0.7	0.9	0.8	0.0	–0.6	–2.1	–2.2	–0.8
		A1B-i2	–2.5	–1.8	–0.6	–1.0	0.0	0.8	0.8	1.0	0.0	–0.8	–2.0	–2.4	–0.7
		A1B-i3	–2.5	–1.8	–0.8	–0.6	–0.2	0.6	1.2	0.8	0.3	–0.8	–1.8	–2.0	–0.6
		A1B-i4	–2.6	–2.3	–1.0	–0.6	–0.1	0.5	0.9	0.6	0.0	–0.9	–2.0	–2.6	–0.8
	CNRM-CM3	A1B-i1	–0.6	–1.2	–2.5	–4.7	–5.3	–5.2	–3.4	–1.4	–1.9	–1.6	–0.5	–0.2	–2.4
	GFDL CM2.1	A1B-i1	–2.3	–1.1	–0.4	0.4	0.5	1.1	2.6	2.6	0.1	–2.1	–2.9	–2.9	–0.4
	ECHAM5/MPI-OM	A1B-i1	–0.1	0.2	0.0	–1.3	–1.6	–2.3	–2.3	–1.9	–1.7	–0.8	–0.2	0.0	–1.0
		A1B-i2	0.0	0.4	0.2	–0.8	–1.5	–2.1	–2.4	–2.1	–1.9	–1.1	–0.2	–0.3	–1.0
		A1B-i3	0.2	0.2	–0.2	–1.3	–1.5	–2.1	–2.3	–2.1	–1.8	–1.0	–0.4	–0.1	–1.0
	CCSM3.0	A1B-i1	–1.5	–1.3	–1.2	–1.6	–1.8	–0.8	0.7	0.4	–1.1	–1.7	–1.9	–1.2	–1.1
		A1B-i2	–1.5	–1.3	–1.4	–2.1	–1.5	0.0	0.7	0.1	–1.0	–1.9	–1.9	–1.5	–1.1
		A1B-i3	–1.4	–1.3	–0.9	–1.8	–1.4	–0.5	0.7	0.0	–1.2	–1.9	–1.8	–1.4	–1.1
		A1B-i4	–1.1	–1.6	–1.5	–2.2	–1.7	–1.0	0.3	0.1	–1.3	–1.7	–1.2	–1.3	–1.2
		A1B-i5	–1.7	–1.2	–1.4	–1.8	–1.3	–0.5	0.8	0.1	–1.2	–1.5	–1.4	–1.3	–1.0
		A1B-i6	–1.6	–1.5	–1.6	–1.9	–1.6	–0.8	0.1	0.4	–1.3	–2.1	–1.5	–1.5	–1.2
	EMR16-A1B		–1.3	–1.0	–0.9	–1.5	–1.4	–0.9	–0.1	–0.1	–0.9	–1.3	–1.3	–1.2	–1.0

Table 3. Contiued.

b)		Realisation	Jan	Feb	Mar	Apr	May	June	Jul	Aug	Sep	Oct	Nov	Dec	Annual
Precipitation (Bias, %)	BCM	A1B-i1	48	60	–4	106	68	–32	–22	193	324	83	142	84	74
	CGCM3.1	A1B-i1	–27	–42	3	184	642	434	29	35	–14	–52	–37	–20	–7
		A1B-i2	–42	–34	5	207	467	295	4	3	–11	–51	–38	–18	–11
		A1B-i3	–22	–40	2	193	550	351	41	19	17	–42	–37	–31	–8
		A1B-i4	–26	–29	–19	164	510	531	48	56	2	–41	–36	–20	–8
	CNRM-CM3	A1B-i1	–9	–18	–31	30	140	499	492	664	550	112	38	29	27
	GFDL CM2.1	A1B-i1	–83	–81	–73	–85	–7	–96	–100	–81	–86	–81	–80	–78	–79
	ECHAM5/ MPI-OM	A1B-i1	–57	–48	–44	–52	–54	84	285	277	11	–73	–59	–45	–49
		A1B-i2	–54	–37	–54	–41	–49	53	326	274	9	–60	–64	–40	–46
		A1B-i3	–31	–54	–57	–31	–60	42	275	186	14	–52	–44	–44	–42
	CCSM3.0	A1B-i1	–46	–56	–44	–21	41	165	377	452	436	2	–40	–42	–31
		A1B-i2	–42	–48	–55	–17	13	92	192	403	323	27	–46	–27	–29
		A1B-i3	–43	–53	–57	–35	16	165	286	385	217	–22	–51	–55	–41
		A1B-i4	–48	–40	–52	–25	9	189	271	409	307	17	–57	–35	–32
		A1B-i5	–38	–49	–42	–21	20	220	253	415	451	30	–49	–36	–26
		A1B-i6	–51	–44	–45	–16	32	249	259	320	421	2	–45	–43	–31
	EMR16-A1B		–36	–38	–36	34	146	202	188	251	186	–13	–31	–26	–21

Table 3. Contiued.

c)		Realisation	Jan	Feb	Mar	Apr	May	June	Jul	Aug	Sep	Oct	Nov	Dec	Annual
Sea level pressure (E)	BCM	A1B-i1	–0.7	–0.6	–1.0	–2.1	–0.9	–1.1	–4.5	–3.2	–5.1	–2.8	–3.6	–3.9	0.6
	CGCM3.1	A1B-i1	–0.9	–2.5	0.0	–3.8	–1.7	–4.0	–1.2	–1.0	–1.7	–4.6	–5.0	–1.3	0.6
		A1B-i2	–0.2	–0.5	–1.5	–2.9	–1.7	–2.2	–1.4	–3.3	–3.1	–2.9	–3.9	–1.1	0.7
		A1B-i3	–0.4	–1.9	–1.2	–2.1	–1.3	–2.7	–0.1	–1.2	–1.3	–3.5	–3.7	–0.5	0.7
		A1B-i4	–1.1	–2.1	–1.0	–1.5	–3.2	–3.2	–1.5	–1.6	–0.6	–2.9	–4.9	–1.1	0.6
	CNRM-CM3	A1B-i1	–1.1	–0.5	–0.7	–1.1	–1.6	–1.9	–4.0	–12.8	–4.6	–1.0	–1.6	–2.5	0.1
	GFDL CM2.1	A1B-i1	–0.8	–2.5	–2.2	–2.1	–1.0	–1.5	–3.2	–5.3	–4.2	–3.9	–3.4	–2.6	0.4
	ECHAM5/ MPI-OM	A1B-i1	–0.1	–1.0	–0.2	–3.3	–1.5	–3.3	–2.8	–4.1	–2.9	–2.0	–1.6	–4.6	0.7
		A1B-i2	–1.1	–0.8	–1.1	–1.4	–0.8	–3.6	–1.7	–3.4	–3.4	–2.2	–1.6	–5.4	0.7
		A1B-i3	–1.0	–0.9	–1.2	–1.6	–1.8	–2.6	–1.2	–2.8	–2.3	–3.2	–2.4	–3.5	0.7
	CCSM3.0	A1B-i1	–2.0	–2.6	–1.7	–3.5	–2.9	–3.9	–0.9	–3.5	–3.4	–7.2	–0.9	–4.1	0.4
		A1B-i2	–2.1	–2.5	–0.7	–2.4	–1.7	–4.8	–1.2	–8.1	–5.0	–4.5	–3.4	–2.9	0.4
		A1B-i3	–1.7	–1.3	–2.7	–1.9	–2.6	–3.9	–1.1	–3.7	–3.1	–6.9	–2.3	–4.9	0.3
		A1B-i4	–1.7	–2.7	–2.2	–5.5	–2.9	–2.0	–4.2	–3.6	–4.8	–3.2	–2.9	–2.7	0.4
		A1B-i5	–1.8	–2.9	–3.0	–3.8	–0.8	–2.7	–1.2	–4.1	–4.0	–7.1	–6.0	–5.5	0.3
		A1B-i6	–1.2	–3.4	–1.1	–3.5	–1.1	–5.5	–3.3	–2.6	–6.7	–4.7	–2.0	–4.1	0.3
	EMR16-A1B		–0.1	–0.3	0.2	–0.4	0.1	–0.1	0.1	–0.3	0.0	–0.2	–0.3	–0.2	0.8

Future climate change

In this section, all realisations of the CGCM3.1 model for scenarios A1B, B1, and A2 together with EMR16-A1B, the ensemble mean of all seven realisations of the B1 scenario (EMR7-B1), and the ensemble mean of all eight realisations of the A2 scenario (EMR8-A2), are used to describe future climate uncertainties for the EMC region (Tab. 1 and Fig. 7).

A. 2-m air temperature

All used scenarios indicate a significant increase in T_{2m} over the EMC between the end of the 1981–2010 reference period and 2071–2100. CGCM3.1-A2 and EMR8-A2 simulations project the highest warming of approximately 2.7 °C and 2.4 °C, respectively, while four realisations of CGCM3.1 for the A1B scenario and EMR16-A1B project a moderate warming of 1.7–1.9 °C. Four realisations of CGCM3.1 for the B1 scenario and EMR7-B1 project the lowest warming of 0.7–1.2 °C.

From 2071–2100 to 2161–2190, T_{2m} is projected to increase slightly over the EMC by between 0.1 °C (CGCM3.1-B1-i1) and 0.8 °C (EMR16-A1B).

B. Total precipitation

From the end of the reference period to 2071–2100, eight of nine used realisations projected a significant decrease in P ranging from 0.11 mm day^{-1} (CGCM3.1-A1B-i4) to 0.04 mm day^{-1} (CGCM3.1-A1B-i1 and CGCM3.1-B1-i4). The EMR16-A1B, EMR8-A2, and EMR7-B1 simulations projected significant decreases of 0.07, 0.06, and 0.04 mm day^{-1}, respectively, while the CGCM3.1-B1-i3 model projected insignificant change in P throughout the studied future period.

From 2071–2100 to 2161–2190, five of seven used realisations of the A1B and B1 scenarios together with EMR16-A1B and EMR7-B1 simulations projected insignificant change in P; CGCM3.1-B1-i2 projected a significant increase of approximately 0.03 mm day^{-1} and CGCM3.1-A1B-i2 a significant decrease of about 0.03 mm day^{-1}.

C. Sea level pressure

Only A1B and A2 scenarios were used in the available GCMs to project *SLP*. In the current century, three of five used realisations together with EMR16-A1B projected insignificant change in *SLP* values, while EMR8-A2, CGCM3.1-A1B-i4, and CGCM3.1-A2 projected smaller decreases of 0.3, 0.4, and 0.6 mbar century^{-1}, respectively. For the following century, all the used realisations and EMR16-A1B projected insignificant change in *SLP* values.

Generally, significant seasonal changes in warming, drought, and the *SLP* system are projected over the study area (data not shown) in the current century:

– For the A1B scenario, EMR16-A1B projected seasonal warming (drought) ranging from 1.9 °C century^{-1} (non-significant tendencies) in summer to 1.5 °C cen-

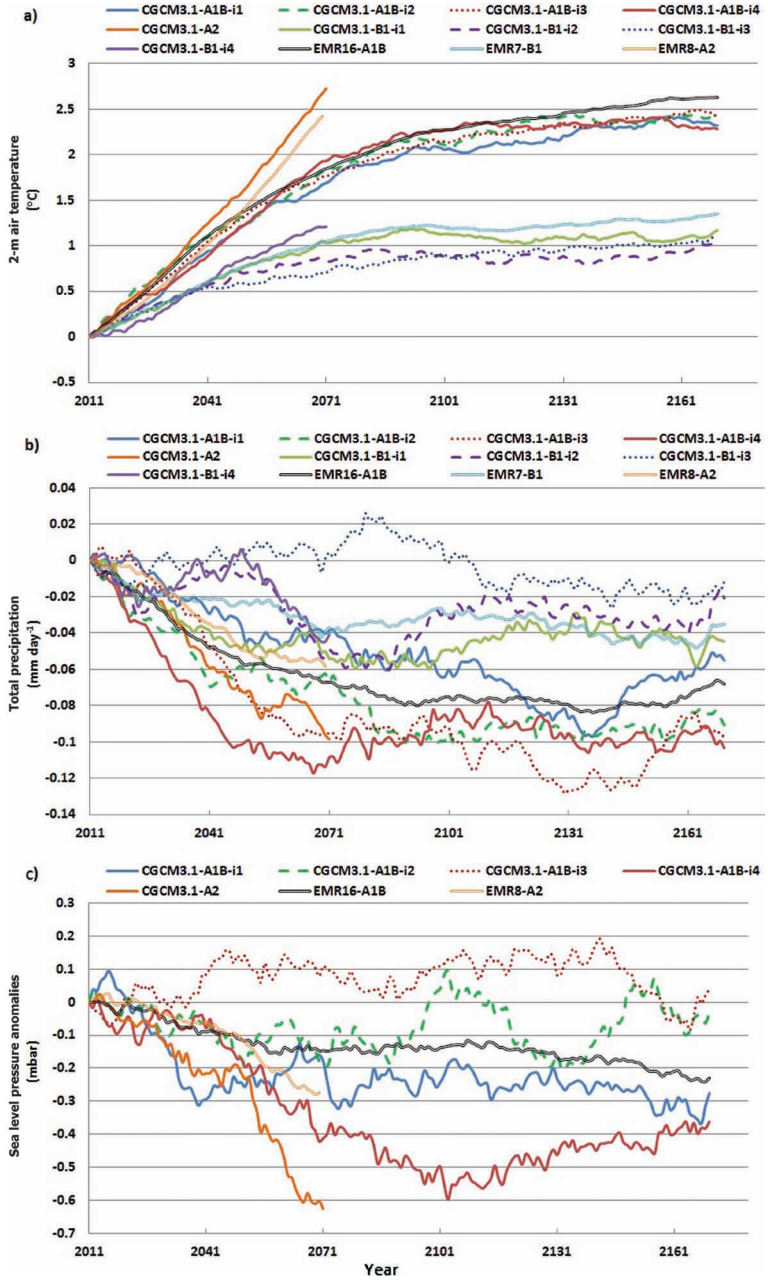

Figure 7. Thirty-year running annual means for (a) 2-m air temperature, (b) total precipitation, and (c) sea level pressure anomalies with reference to the 1981–2010 averages for various GCM scenarios (no B1 scenario for sea level pressure). (The results of the Global Climate models are used to calculate the characteristics of the reference period)

tury^{-1} (–0.1 mm day^{-1} century^{-1}) in winter. The seasonal variability of the *SLP* linear trend would range from –1.17 mbar century^{-1} in summer to 0.81 mbar century^{-1} in winter.

– For the A2 scenario, EMR8-A2 projected a seasonal warming trend ranging from 2.9 °C century^{-1} in summer to 2 °C century^{-1} in winter. The seasonal variability of the *P* (*SLP*) linear trend would range from non-significant tendencies (–1.53 mbar century^{-1}) in summer to –0.12 mm day^{-1} century^{-1} (0.83 mbar century^{-1}) in winter.

– For the B1 scenario, EMR7-B1 projected a seasonal warming trend ranging from 1.3 °C century^{-1} in spring to 1 °C century^{-1} in winter and autumn. This simulation projected seasonal variability of the *P* linear trend ranging from non-significant (summer) to –0.06 mm day^{-1} century^{-1} (winter and spring).

4. Summary and conclusion

The studied reanalysis data were significantly correlated with independent observations, with a regression slope significantly equal to one. Standard statistical tests (i.e., *t*- and *f*-tests) indicated similar distributions of mean and variance values, indicating that the ERA-Interim data can be used to characterize the present EMC climate.

The values of individual weather variable averages and trends together with regression comparisons are shown in the figures and tables. Air warming together with decreasing precipitation rates and *SLP* are the important changes characterising the future EMC climate. During the 1979–2010 period, ERA-Interim data indicated that the annual average values (trend) of air temperature, total precipitation, and *SLP* would be 20.56 ± 5.3 °C (0.5 °C decade^{-1}), 0.432 ± 1.35 mm day^{-1} (–0.03 mm day^{-1} decade^{-1}), and 1014.26 ± 5 mbar (–0.3 mbar decade^{-1}), respectively. The trends and annual average values for the studied weather variables over the last three decades display particular spatial, hourly, and seasonal distributions along the study area. The 2-m air temperature, *SLP*, and total precipitation are clearly linked with the NAO Index.

Air temperature increased towards the south, except in the eastern part of the EMC, while SLP increased towards the west. Precipitation is significantly greater in the north than the south and in the east than the west, which means that the study area is subject to four precipitation regimes, in agreement with Hafez and Hasanean (2000). The precipitation pattern will probably display a climate shift towards an extremely wet season.

During the 1979–2010 study period, *SLP* is the climate variable displaying the lowest interannual variability. Air temperature at 2 m also displays low interannual variability, possibly due to the moderating effect of the Mediterranean Sea, which reduces temperature variability. Total precipitation displays high interannual variability. *SLP* and 2-m air temperature display high (low) seasonal variability in winter (summer) time.

In the third part of the paper, future climate change uncertainties in terms of T_{2m}, P, and SLP are described over the EMC based on six GCMs. Based on comparing the ERA-Interim reanalysis data with the results of six GCM realisations of the A1B scenario during the control period, four CGCM3.1 model realisations of the A1B scenario together with the ensemble mean of all 16 realisations of the A1B scenario are found to be the best available simulations describing the current EMC climate.

Generally, in the current century, there is projected to be a significant increase in the annual average T_{2m} ranging from 0.7–1.1 °C (B1 scenario) to 1.7–2 °C (A1B scenario) and 2.4–2.7 °C (A2 scenario), most markedly in summer. This warming was in good agreement with that predicted in the IPCC (2007) report, but less than the global warming of 0.6 °C predicted by Arnell (2004) and less than the northern Mediterranean region warming of 0.4 °C predicted by Alcamo et al. (2007), partly because the study area is a coastal region. Moreover, P was projected to decrease significantly, by 0.11–0.04 mm day^{-1}, with the A1B and A2 emission scenarios, most markedly in winter; on the other hand, the B1 scenario projected an insignificant change. The substantial droughts projected for the study area agree with the IPCC (2007) report predictions and with the results of Goubanova and Li (2007) and Giorgi and Lionello (2008). For SLP, the results of the A2 scenario indicate a small decrease while those of the A1B scenario indicate insignificant change.

The EMC area is exposed to climate change, and its responses in terms of T_{2m}, P, and SLP are now better understood. This information will constitute a useful database with which to improve the adaptation tools needed to address the area's climate change problems by 2200. Moreover this information can be used to forecast the oceanic conditions in the EMC region for the coming 100 years, using a coupled ocean–atmosphere model. The projection of oceanic conditions, especially sea level rise, is one of the most important climate change tasks. Sea level rise would significantly harm much of the Egyptian Mediterranean coast, which is only 2 m above the mean sea level, by submerging and destroying its protective sand belt.

The conclusions of the present work can be summarized as follows:

– The Egyptian Mediterranean coast climate is expected to change dramatically by the end of the current century, with especially dramatic changes in terms of warming and increased drought conditions.

– The potential effects of climate change are expected to have many socio-economic impacts, changing, for example, agricultural patterns and water demand. Moreover, the spatial and temporal distribution of different weather variable trends will affect the present balance between water resources and demand and between crop production and needed temperatures and water.

– In addition, climate change may affect the marine systems by changing sea waves and current systems together with navigational channels and the sea

level. The Egyptian government and citizens need to work together to find adaptation solutions to address change in the Egyptian Mediterranean coast climate.

Acknowledgements – This work was done when Dr. Shaltout was a post-doctoral researcher at the Ocean Climate Group, Department of Earth Sciences, University of Gothenburg, Sweden, under the auspices of the Swedish Institute Guest Scholarship Program. We would also like to thank Stephen Sanborn at Proper English AB for the English language editing.

References

Accadia, A., Mariani, S. and Casaioli, M. (2005): Verification of precipitation forecasts from two limited-area models over Italy and comparison with ECMWF forecasts using a resampling technique, *Weather Forecast.*, **20**, 276–300.

Agrawala, S., Moehner, A., El Raey, M., Conway, D., van Aalst, M., Hagenstad, M. and Smith, J. (2004): *Development and climate change in Egypt: Focus on coastal resources and the Nile*. Organization for Economic Co-operation and Development (OECD), Working party on global and structural policies and Working party on development co-operation and Eenvironment, Paris, France [Available online from http://www.oecd.org/dataoecd/57/4/33330510.pdf].

Alcamo, J., Moreno, J. M., Novaky, B., Bindi, M., Corobov, R., Devoy, R. J. N, Giannakopoulos, C., Martin, E., Olesen, J. E. and Shvidenko, A. (2007). Europe. Climate Change 2007: Impacts, adaptation and vulnerability. Contribution of Working group II to the Fourth assessment report of the Intergovernmental panel on climate change, edited by Parry, M. L., Canziani, O. F., Palutikof, J. P., van der Linden, P. J., and Hanson, C. E., Cambridge University Press, Cambridge, UK, 541–580.

Arnell, N. W. (2004): Climate change and global water resources: SRES emissions and socio-economic scenarios, *Global Environ. Chang.*, **14**, 31–52.

Berrisford, P., Dee, D., Poli, P., Brugge, R., Fielding, K., Fuentes, M., Kallberg, P., Kobayashi, S., Uppala, S. and Simmons, A. (2011): The ERA-Interim archive, version 2.0. ERA report series. **1** (Technical report), ECMWF, 23 pp.

Cherubini, T., Ghelli, A. and Lalaurette, F. (2002): Verification of precipitation forecasts over the Alpine region using a high-density observing network, *Weather Forecast.*, **17**, 238–249.

Collins, W. D., Bitz, C. M., Blackmon, M. L., Bonan, G. B., Bretherton, C. S., Carton, J. A., Chang, P., Doney, S. C., Hack, J. J., Henderson, T. B., Kiehl, J. T., Large, W. G., McKenna, D. S., Santer, B. D. and Smith, R. D. (2006): The community climate system model: CCSM3, *J. Climate*, **19**, 2122–2143.

Delworth, T. L., Broccoli, A. J., Rosati, A., Stouffer, R. J., Balaji, V., Beesley, J. T., Cooke, W. F., Dixon, K. W., Dunne, J., Dunne, K. A., Durachta, J. W., Findell, K. L., Ginoux, P., Gnanadesikan, A., Gordon, C. T., Griffies, S. M., Gudgel, R., Harrison, M. J., Held, I. M., Hemler, R. S., Horowitz, L. W., Klein, S. A., Knutson, T. R., Kushner, P. J., Langenhorst, A. L., Lee, H.-C., Lin, S. J., Lu, J., Malyshev, S. L., Milly, P. C., Ramaswamy, V., Russell, J., Schwarzkopf, M. D., Shevliakova, E., Sirutis, J., Spelman, M., Stern, W. F., Winton, M., Wittenberg, A. T., Wyman, B., Zeng, F. and Zhang, R. (2006): GFDL's CM2 global coupled climate models – Part 1: Formulation and simulation characteristics, *J. Climate*, **19**, 643–674.

Deque, M., Dreveton, C., Braun, A. and Cariolle, D. (1994): The ARPEGE/IFS atmosphere model, *Clim. Dynam.*, **10**, 249–266.

Domroes, M. and El-Tantawi, A. (2005): Recent temporal and spatial temperature changes in Egypt, *Int. J. Climatol.*, **25**, 51–63.

Douglas, E. M., Beltrán-Przekurat, A., Niyogi, D., Pielke, R. A. and Vörösmarty, C. J. (2009): The impact of agricultural intensification and irrigation on land–atmosphere interactions and Indian monsoon precipitation – A mesoscale modeling perspective, *Global Planet. Change*, **67**, 117–128.

Flato, G. M. (2005): The third generation coupled global climate model (CGCM3) [Available online from http://www.cccma.bc.ec.gc.ca/models/cgcm3.shtml].

Giorgi, F., and Lionello, P. (2008): Climate change projections for the Mediterranean region, *Global Planet. Change*, **63**, 90–104.

Goubanova, K. and Li, L. (2007): Extremes in temperature and precipitation around the Mediterranean basin in an ensemble of future climate scenario simulations, *Global Planet. Change*, **57**, 27–42.

Hafez, Y. Y. and Hasanean, H. M. (2000): The variability of winter time precipitation in the Northern coast of Egypt and its relationship with the North Atlantic oscillation, ICEHM2000, 9–12 September 2000, Cairo University, Egypt, 175–186.

Hasanean, H. M. (2004a): Winter time surface temperature in Egypt in relation to the associated atmospheric circulation, *Int. J. Climatol.*, 24, 985–999.

Hasanean, H. M. (2004b): Precipitation variability over the Mediterranean and its linkage with El Nino Southern oscillation (ENSO), *J. Meteorol.*, **29**, 151–160.

Hasanean, H. M. and Abdel Basset, H. (2006): Variability of summer temperature over Egypt, *Int. J. Climatol.*, **26**, 1619–1634.

Houghton, J. T., Ding, Y., Griggs, D. J., Noguer, M., van der Linden, P. J., Dai, X, Maskell, K. and Johnson, C. A. (2001): *Climate change 2001: The scientific basis*. Cambridge University Press: Cambridge, 83 pp.

IPCC (2000): Special report (emissions scenarios). Summary for policymaker of working group III, ISBN: 92-9169-113-5, 27 pp.

IPCC (2007): Climate change 2007: Synthesis report. Contribution of working groups I–III to the Fourth assessment report of the Intergovernmental panel on climate change, Cambridge University Press, Cambridge.

Jungclaus, J. H., Botzet, M., Haak, H., Keenlyside, N., Luo, J., Latif, M., Marotzke, J., Mikolajewicz, U. and Roeckner, E. (2006): Ocean circulation and tropical variability in the coupled model ECHAM5/MPI-OM, *J. Climate*, **19**, 3952–3972.

Kaltenbrock, R., Diendorfer, G. and Dotzek, N. (2009): Evaluation of thunderstorm indices from ECMWF analyses, lightning data and severe storm reports, *Atmos. Res.*, **93**, 381–396.

Kjellström, E. M., Grigory, N., Hansson, U., Strandberg, G. and Ullerstig, A. (2011): 21st century changes in the European climate: Uncertainties derived from an ensemble of regional climate model simulations, *Tellus*, **63A**, 24–40.

Räisänen, J. and Alexandersson, H. (2003): A probabilistic view on recent and near future climate change in Sweden, *Tellus*, **55A**, 113–125.

Scavia, D., Field, J. C., Boesch, D. F., Buddemeier, R. W., Burkett, V., Cayan, D. R., Fogarty, M., Harwell, M., Howarth, R. W., Mason, C., Reed, D. J., Royer, T., Salinger, A. H. and Titus, J. G. (2002): Climate change impacts on U.S. coastal and marine ecosystems, *Estuaries*, **25**, 149–164.

Terray, L., Valcke, S. and Piacentini, A. (1998): *OASIS 2.2 Guide and reference manual*. Technical report TR/CMGC/98-05, Centre Européen de Recherche et de Formation Avancée en Calcul Scientifique, Toulouse, France.

UNDP (2007): Human Development Report 2007–2008: Fighting Climate Change: Human Solidarity in a Divided World. Palgrave Macmillan, New York. UNDP-2, Poverty Eradication, MDGs and Climate Change. UNDP, Environment.

SAŽETAK

Recentni klimatski trendovi i budući scenariji duž egipatske obale Sredozemlja

Mohamed Shaltout, Ahmed El Gindy i Anders Omstedt

Ovaj rad analizira sadašnju klimu mediteranskog obalnog područja Egipta (EMC) i odziv odgovarajućih klimatskih varijabli na globalne promjene. Ispitano je podudaranje ERA-Interim baze podataka za razdoblje 1979–2010 za promatrano područje s raspoloživim podacima neovisnih opažanja. Nadalje, usporedbom s ERA-Interim bazom podataka ispitana je pouzdanost šest globalnih klimatskih modela (GCM), zajedno sa srednjakom ansambla višestrukih modelskih realizacija A1B scenarija. Konačno, GCM simulacije su korištene za opisivanje nepouzdanosti u budućoj promjeni klime duž EMC-a.

Rezultati pokazuju da se opažanja dobro slažu s ERA-Interim podacima. Podaci za EMC u razdoblju 1979–2010 ukazuju na signifikantni pozitivni trend temperature zraka na 2 m visine, koji je popraćen signifikantnim negativnim trendovima ukupne oborine i tlaka zraka na morskoj razini. Klimatski model koji najbolje opisuje sadašnju EMC klimu je CGCM 3.1, koji je upotrebljen za opisivanje buduće klime razmatranog područja. Model CGCM 3.1 ukazuje na to da EMC područje krajem ovog stoljeća očekuje signifikantno zatopljenje uz značajne suše i blago smanjenje tlaka zraka na razini mora.

Ključne riječi: Sredozemno more, Egipat, temperatura zraka, oborina, tlak zraka na razini mora, klima, analiza trenda, klimatski modeli

Corresponding author's address: Mohamed Shaltout, currently research scientist at Department of Earth Sciences, University of Gothenburg, Göteborg, Sweden. P. O. Box 460, 40530 Gothenburg, Sweden, tel: +46 31 78 62 859, e-mail: mohamed.shaltout@gvc.gu.se